Acta Biochim Biophys Sin xxxx, xx(xx): xx–xx
https://cstr.cn/32197.14.abbs.2026057
https://doi.org/10.3724/abbs.2026057
Original Article

Original Article

Shikonin sensitises osimertinib-resistant lung adenocarcinoma to ferroptosis through HES1-mediated ATF3 upregulation

Haiwen Li[1,2,3,4,†], Quan Yang[1,3,4,†], Li Yang[1,2,3,4,†], Xiaobi Huang[1,3,4], Yongyang Chen[1,3,4], Yonghua Chen[6], Yuexin Zheng[1], Xiao Lei[1], Miao Yin[1], Yuetong Jiang[1], Yudong Guo[1], Yanfeng Liang[1], Qihe Long[1], Zhixiong Yang[1], Lili Yu[2,5,*], and Wenmei Su[1,2,3,4,*]

[1]Department of Pulmonary Oncology, Affiliated Hospital of Guangdong Medical University, Zhanjiang 524000, China, [2]Faculty of Chinese Medicine, Macau University of Science and Technology, Macau 999078, China, [3]Guangdong Provincial Key Laboratory of Autophagy and Major Chronic Non-communicable Diseases, Affiliated Hospital of Guangdong Medical University, Zhanjiang 524000, China, [4]Zhanjiang Key Laboratory of Tumor Microenvironment and Organoid Research, Zhanjiang 524000, China, [5]The State Key Laboratory for Quality Research in Chinese Medicines of the Macau University of Science and Technology, Macau 999078, China, and [6]Department of Pathological Diagnosis and Research Center, Affiliated Hospital of Guangdong Medical University, Zhanjiang 524000, China

[†]These authors contributed equally to this work.

*Correspondence address. E-mail: llyu@must.edu.mo (L.Y.); suwenmei123@hotmail.com (W.S.)

Received 28 October 2025 Accepted 24 March 2026 Published 8 July 2026

Abstract

Acquired resistance to osimertinib poses a major challenge in treating EGFR-mutant lung adenocarcinoma (LUAD). Here, we demonstrate that shikonin, a natural compound from *Lithospermum erythrorhizon*, synergizes with osimertinib to overcome this resistance by inducing ferroptosis. In osimertinib-resistant LUAD cells (PC9-OR/H1975-OR), the shikonin-osimertinib combination significantly enhances cytotoxicity and suppresses proliferation while triggering ferroptotic events, including reactive oxygen species accumulation, lipid peroxidation, and iron overload alongside glutathione depletion. RNA-sequencing identifies Hes family BHLH transcription factor 1 (HES1) downregulation as crucial to this process. *HES1* knockdown replicates the combination's effects. Mechanistically, *ATF3* is identified as a direct transcriptional target of HES1, with HES1 binding to the *ATF3* promoter (–786 to –779 nt) to repress its transcription. The shikonin-osimertinib combination relieves this repression, leading to ATF3-mediated suppression of the ferroptosis regulators SLC7A11 and GPX4. *In vivo*, this combination potently inhibits tumor growth in xenograft models without observable toxicity. Our study reveals a novel HES1/ATF3 axis governing ferroptosis and proposes shikonin as a promising therapeutic adjuvant to overcome osimertinib resistance in LUAD.

Key words shikonin, osimertinib, lung adenocarcinomas, ferroptosis, HES1, ATF3

Introduction

Lung adenocarcinoma (LUAD), the most prevalent subtype of non-small cell lung cancer (NSCLC), remains a leading cause of cancer-related mortality worldwide [1]. For patients with advanced EGFR-mutant LUAD, epidermal growth factor receptor tyrosine kinase inhibitors (EGFR-TKIs), particularly the third-generation agent osimertinib, have become a standard first-line treatment [2,3]. Although osimertinib significantly improves progression-free survival and overall survival [4–6], the development of acquired resistance inevitably limits its long-term efficacy, creating a pressing need for novel strategies to restore therapeutic sensitivity [7].

In the search for such strategies, natural products derived from Traditional Chinese Medicine (TCM) have attracted growing interest for their potential to reverse cancer drug resistance. Among them, shikonin, a bioactive naphthoquinone isolated from *Lithospermum erythrorhizon* (Zicao) plant, has demonstrated broad-

© The Author(s) 2026. This is an open access article distributed under the terms of the Creative Commons Attribution License (https://creativecommons.org/licenses/by/4.0/).

spectrum antitumor activity [8–11] by inducing multiple forms of regulated cell death, including apoptosis [12,13], necroptosis [14], and ferroptosis [8]. Notably, shikonin can synergize with conventional chemotherapeutics such as cisplatin, gemcitabine and doxorubicin to reverse multidrug resistance [15–18]; however, its potential role in modulating osimertinib resistance has not yet been investigated.

Another promising avenue for overcoming drug resistance lies in the induction of ferroptosis, an iron-dependent form of regulated cell death driven by lipid peroxidation and redox imbalance [19–21]. Accumulating evidence suggests that targeting ferroptosis may enhance the efficacy of conventional cancer therapies, including chemotherapy, immunotherapy, and targeted agents [22]. This approach is particularly relevant in osimertinib-resistant LUAD, as demonstrated by agents such as Dauricine, which overcome resistance by inducing ferroptosis through novel mechanisms such as SAT1 stabilization [23]. Beyond newly identified regulators such as SAT1, the core ferroptosis machinery is well-established, including SLC7A11 and GPX4, which maintain redox homeostasis, and ATF3, a stress-responsive transcription factor that suppresses SLC7A11 to promote ferroptosis [24,25]. We therefore sought to investigate whether other transcription factors implicated in lung cancer progression might similarly regulate this process. Intriguingly, the Notch effector HES1 (Hes family BHLH transcription factor 1), a transcriptional repressor frequently overexpressed in LUAD, has been associated with chemotherapy resistance and poor prognosis [26], yet its potential role in ferroptosis remains unclear.

Based on these observations, we hypothesized that shikonin can overcome osimertinib resistance by targeting HES1-mediated suppression of ferroptosis. Using *in vitro* and *in vivo* models of osimertinib-resistant LUAD, we demonstrated that shikonin synergizes with osimertinib to induce ferroptosis via HES1 downregulation, which in turn relieves ATF3 transcriptional repression and subsequently inhibits SLC7A11/GPX4 expressions. Our findings revealed a previously unrecognized mechanism of osimertinib resistance and provided a compelling rationale for combining shikonin with EGFR-TKIs to improve LUAD treatment.

Materials and Methods

Materials

Osimertinib (HY-15772), shikonin (HY-N0822), erastin (HY15763), Z-VAD-FMK (HY16658B), ferrostatin-1 (Fer-1; HY100579), 3-methyladenine (3-MA; HY19312), and deferoxamine mesylate (DFO; HYB0988) were purchased from MedChemExpress (Shanghai, China). For our assays, we used FerroOrange (F374; Dojindo, Tokyo, Japan), BODIPY 581/591 C11 probe, ROS Assay kit, GSH Assay kit, BCA Protein Assay kit, and MDA Assay kit, all of which were obtained from Beyotime (Shanghai, China). Lipofectamine 3000, and Opti-MEM were obtained from Thermo Fisher Scientific (Waltham, USA). Plasmids containing the HES1 or ATF3 inserts were obtained from GeneChem (Shanghai, China). Primary antibodies targeting HES1 (11988S), ATF3 (18665S), SLC7A11 (12691S), and GPX4 (59735S) were obtained from Cell Signaling Technology (Danvers, USA).

Cell lines and culture conditions

Human LUAD cell lines PC9 and H1975 and human embryonic kidney 293T cells were obtained from the American Type Culture Collection (ATCC; Manassas, USA). The osimertinib-resistant LUAD cell lines PC9-OR and H1975-OR were established in our laboratory as previously reported [23,27]. LUAD cells were cultured in RPMI 1640 (Gibco, Carlsbad, USA), and 293T cells were grown in DMEM (Gibco) with 10% fetal bovine serum (FBS) and 1% penicillin-streptomycin (Gibco) at 37°C in a 5% CO_2 atmosphere. Cell line authentication (STR profiling) and mycoplasma testing were performed every quarter.

Cell viability assay

PC9, PC9-OR, H1975, and H1975-OR cells were plated in 96-well plates at a density of 5000 cells per well. After 24 h of attachment, cells were exposed to osimertinib (0, 4, 8, 16, or 32 μM), shikonin (0, 0.5, 1, 2, 4, or 8 μM), Z-VAD-FMK (10 μM), 3-MA (50 μM), Fer-1 (5 μM), DFO (5 μM), erastin (5 μM), or mixtures of these agents for 48 h. Drug concentrations were selected based on preliminary IC_{50} determinations. The experimental groups were treated as follows: control (0 μM), osimertinib (PC9-OR: 16 μM; H1975-OR: 12 μM), shikonin (1 μM), and their combination (PC9-OR: 16 μM osimertinib + 1 μM shikonin; H1975-OR: 12 μM osimertinib + 1 μM shikonin). For siRNA experiments, cells were transfected with HES1-specific siRNAs (siHES1-1 and siHES1-2) and siHES1-NC using Lipofectamine 2000 (Invitrogen, Carlsbad, USA) for 48 h, followed by osimertinib treatment for 24 h. The WST-1 assay was used to examine cell viability according to the manufacturer's protocol, and absorbance was measured using a microplate reader (Epoch; BioTek, Winooski, USA).

Colony formation assay

PC9-OR and H1975-OR cells were treated with various drugs or transfected with siHES1-1, siHES1-2, or siHES1-NC for 48 h and then reseeded at 500 cells/well in 6-well plates. After a 14-day incubation period, the cells were fixed using a 4% paraformaldehyde solution and stained with 1% crystal violet, and colonies consisting of more than 50 cells were counted.

Cell apoptosis assay

PC9-OR and H1975-OR cells were treated with osimertinib, shikonin, or a combination of both for 48 h. After treatment, cells were collected by trypsinization, washed twice with cold PBS, and resuspended in 1× binding buffer. Cells were then stained with Annexin V-FITC/PI using the Apoptosis Detection kit (Beyotime) and analyzed using flow cytometry within 1 h. Data analysis was performed using FlowJo software (version 10.8.1), with early and late apoptotic populations quantified.

Total ROS assay

Following a 48-h exposure to osimertinib, shikonin, or their combination, the cells were collected and washed with PBS. Subsequently, they were incubated with 10 μM DCFH-DA in serum-free medium at 37°C for 30 min in the dark. After incubation, the cells were washed twice with PBS and evaluated using flow cytometry. A minimum of 10,000 events were recorded per sample, and the mean fluorescence intensity was used for statistical analysis.

Lipid ROS assay

Cells were seeded in culture plates and exposed to the specified agents. After incubation, the cells were rinsed with PBS, followed by a 30-min incubation with C11-BODIPY in serum-free medium at 37°C. Subsequently, the cells were washed again with serum-free

medium, resuspended, and analyzed using flow cytometry to determine the fluorescence intensity indicative of the lipid ROS levels.

MDA assay

Cells were seeded in culture dishes and subjected to specified treatments. After incubation, the cells were lysed with cell lysis buffer on ice for 15 min. The supernatant was then centrifuged and collected. The protein concentration was measured using a BCA Protein Assay kit. The samples were heated at 100°C for 15 min. Finally, a microplate reader was used to measure absorbance at 532 nm to assess MDA levels.

GSH assay

Cells were collected, washed, and lysed to measure GSH using a protein removal reagent. Protein quantification and GSH levels were assessed using a Total GSH Assay kit. At 25°C, the absorbance was measured at 412 nm, and the GSH content was calculated using standard curves.

Intracellular iron assay

The cells were cultivated in 12-well plates and treated as needed. After treatment, the cells were washed with PBS and incubated with 1 μM FerroOrange probe for 30 min at 37°C in a 5% CO_2 incubator. The cells were directly observed and imaged without washing using a BioTek Cytation 5™ Cell Imaging Multi-Mode Reader (BioTek).

RNA-sequencing and analysis

Total RNA was extracted from PC9-OR cells (control and treated groups; $n = 3$) using TRIzol reagent (Invitrogen). RNA quality was verified using an Agilent 2100 Bioanalyzer (RIN > 9.0) (Agilent, Santa Clara, USA). Libraries were prepared with the NEBNext Ultra II kit (New England Biolabs, Ipswich, USA) and quantified by a Qubit fluorometer (Thermo Fisher Scientific). Sequencing was performed on an Illumina NovaSeq 6000 platform (150 bp paired-end reads; Illumina, San Diego, USA). Raw reads were processed with FastQC/Trimmomatic, aligned to GRCh38.p13 (STAR), and counted (feature counts). Differential expression analysis was performed using DESeq2, with DEGs defined as FDR-adjusted $P < 0.001$ and $|\log2FC| > 1$. A volcano plot was generated with ggplot (R version 3.6.1).

Microarray data retrieval

LUAD RNA-seq data were retrieved from the TCGA database (https://portal.gdc.cancer.gov). Paired tumor and adjacent normal tissue samples were selected, and all tumor samples were analyzed for HES1 expression using DESeq2 by Edge R. Samples with high HES1 expression were identified. Survival analysis involved extracting survival time and status from clinical data, with Kaplan-Meier curves generated using the survival and survminer packages. ROC analysis was conducted using the pROC package to assess HES1's diagnostic efficacy, and the AUC was calculated to quantify the accuracy.

Clinical tissue samples

Samples of LUAD and their corresponding normal tissue counterparts were acquired from the Department of Thoracic Surgery at the Affiliated Hospital of Guangdong Medical University in China. Eligible patients were adults aged 18–70 years with newly diagnosed lung adenocarcinoma. Supplementary Table S1 provides detailed clinical information. All patients were enrolled upon voluntary written informed consent, and participation continued unless the patients explicitly withdrew their consent. Ethical approval for this study was granted by the Ethical Committee of the Affiliated Hospital of Guangdong Medical University (approval number: PJKT2024-023).

RNA extraction and quantitative real-time PCR analysis

RNA was extracted from tissues and cells using TRIzol reagent (Invitrogen), according to the manufacturer's guidelines. The extracted RNA was converted to cDNA using a reverse transcription kit (TaKaRa, Dalian, China). Subsequently, Quantitative real-time PCR analysis (RT-qPCR) was conducted to amplify the target genes. *GAPDH* served as an internal control, and the mRNA expression levels of *HES1*, *ATF3*, and *SLC7A11* were quantified using the $2^{-\Delta\Delta Ct}$ method for normalization. The gene-specific primer sequences are presented in Supplementary Table S2.

Western blot analysis

Proteins were extracted using RIPA lysis buffer containing protease and phosphatase inhibitors and quantified using a BCA Protein Assay kit. Equal amounts of protein (20 μg per lane) were separated by 12.5% SDS-PAGE and transferred onto PVDF membranes (Millipore, Billerica, USA) using a wet transfer system. Membranes were blocked with 5% non-fat milk in TBST for 1 h at room temperature. Primary antibodies against HES1, ATF3, SLC7A11, and GPX4 were used at a 1:1000 dilution and incubated overnight at 4°C. After washing with TBST (3 × 10 min), the membranes were incubated with HRP-conjugated secondary antibodies (1:5000) for 1 h at room temperature. Immunoreactive bands were detected using ECL reagents (Zeta Life, Menlo Park, USA), and signals were visualized and recorded using a Tanon 5200 CL imaging system (Tanon, Beijing, China), enabling the analysis and comparison of protein expression levels.

Small interfering RNA (siRNA) and plasmid transfection

For transfection, cells were treated with HES1-/ATF3-specific siRNAs (siRNA-1 and siRNA-2) and siRNA-NC using Lipofectamine 2000. HES1 overexpression plasmids, along with wild-type and mutant ATF3 plasmids, were constructed and introduced into the cells using Lipofectamine 3000. Specific sequences of the siRNAs and plasmids are provided in Supplementary Table S3.

Dual-luciferase reporter gene assay

293T cells overexpressing HES1 or serving as controls were co-transfected with a *Renilla* luciferase reporter vector and GV534-*ATF3*-promoter reporter vector using Lipofectamine 3000 following the manufacturer's protocol outlined by the supplier. After 48 h of incubation post-transfection, the cells were harvested for analysis. The luciferase activity was quantified using a Dual-luciferase Reporter Assay kit (GeneChem, Shanghai, China). To normalize for variations in the transfection efficiency, *Firefly* luciferase readings were adjusted based on the *Renilla* luciferase signal. Normalized luciferase activity, calculated as the ratio of *Firefly* to *Renilla* luminescence, was used to assess the effect of HES1 overexpression on *ATF3* promoter activity.

Chromatin immunoprecipitation assay

PC9-OR cells were cross-linked with 1% formaldehyde for 10 min at

room temperature, and the reaction was quenched with 125 mM glycine. Cells were sonicated to obtain DNA fragments of 200–500 bp. Chromatin was immunoprecipitated using anti-HES1 antibody (11988S; Cell Signaling Technology) or normal rabbit IgG (2729; Cell Signaling Technology) as a negative control. After reversal of cross-links, DNA fragments were extracted from the beads and analyzed by RT-qPCR and agarose gel electrophoresis to ascertain the presence and length of the specific DNA sequences. The entire process was conducted in triplicate to verify the consistency of the results. Primer sequences targeting the *ATF3*, *SLC7A11*, and *GPX4* promoter regions are detailed in Supplementary Table S4.

Nude mouse xenograft model

Twenty-four female BALB/c nude mice (Huachuang Xinnuo, Taizhou, China), aged 4–6 weeks and weighing 18 ± 2 g, were used in this study. PC9-OR cells in the logarithmic growth phase were trypsinized and suspended in 0.2 mL of a 1:1 mixture of PBS and Matrigel, achieving a concentration of 10^6 cells/mL. After disinfecting the left axilla with 75% alcohol, 200 μL of cell suspension was injected. Tumor volume and body weight were measured every three days, and the tumor volume was calculated using the following formula: length × (width^2) × 0.5. Once the tumors reached 80–100 mm^3, the mice were randomly divided into four groups (n = 6 each): control group (saline), osimertinib (5 mg/kg) [28–30], shikonin (0.8 mg/kg) [15,31], and a combination group. On day 22, the mice were euthanized by cervical dislocation, and the tumors were weighed and photographed. All animal experiments were formally reviewed and approved by the Animal Ethics and Welfare Committee of the Affiliated Hospital of Guangdong Medical University (approval number: AHGDMU-LAC-B-202312-0086).

Biomedical measurement

The serum levels of alanine aminotransferase (ALT), aspartate aminotransferase (AST), blood urea nitrogen (BUN), creatinine (CRE), total protein (TP), and albumin (ALB) were assessed using an automated biochemical analyzer, strictly adhering to each kit's protocol to ensure accuracy and consistency in the experimental measurements.

Hematoxylin-eosin and immunohistochemistry

Xenograft tumor tissues were fixed in 4% paraformaldehyde, embedded in paraffin, and sectioned at 4-μm thickness. For immunohistochemistry (IHC), sections were deparaffinized, rehydrated, and subjected to antigen retrieval using citrate buffer (pH 6.0) at 95°C for 20 min. Endogenous peroxidase activity was blocked with 3% H_2O_2 for 15 min. Sections were incubated with primary antibodies against Ki67, HES1, ATF3, and SLC7A11 overnight at 4°C, followed by HRP-conjugated secondary antibodies for 1 h at room temperature. DAB was used as a chromogen, and hematoxylin was used for counterstaining. The protein expression levels were quantitatively evaluated using the H-score method. All slides were evaluated independently by two pathologists blinded to the treatment groups.

Statistical analysis

Statistical evaluation of the data was carried out using GraphPad Prism 8.0, with results depicted as the mean value ± standard deviation (SD). Student's t test was applied to assess statistical significance, and $P < 0.05$ was considered as significantly different. Each experiment was repeated at least three times to ensure reliability.

Results

Synergistic antitumor effects of shikonin and osimertinib in resistant LUAD cells

To investigate potential strategies to overcome osimertinib resistance, we first established resistant cell lines (PC9-OR and H1975-OR) by chronic exposure to increasing concentrations of osimertinib. These resistant cells demonstrated significantly reduced sensitivity compared with their parental counterparts (Supplementary Figure S1A–D). We next evaluated the efficacy of shikonin (Figure 1A) and found that monotherapy exhibited dose-dependent cytotoxicity in both resistant lines, with IC_{50} values of 2.22 μM for PC9-OR and 2.53 μM for H1975-OR (Figure 1B).

Strikingly, the combination of suboptimal doses of shikonin (1 μM) with osimertinib (4–16 μM) resulted in significantly enhanced growth inhibition compared to either agent alone (Figure 1C). Synergy analysis confirmed strong pharmacological synergy, as combination index values were consistently below 1 across multiple dose combinations (Figure 1D).

The synergistic anti-proliferative effect was further substantiated by colony formation assays, which showed that the combination treatment markedly reduced clonogenic survival compared to monotherapy or the control groups (Figure 1E,F). Consistently, flow cytometric analysis confirmed that the combined regimen significantly increased cell death in both resistant cell lines (Figure 1G,H).

Ferroptosis drives synergistic cell death in osimertinib-resistant LUAD cells

To elucidate the mechanism underlying the synergistic cell death, we treated PC9-OR and H1975-OR cells with the shikonin-osimertinib combination in the presence of pathway-specific inhibitors. Cell death was not rescued by Z-VAD-FMK or 3-MA ($P > 0.05$) but was significantly attenuated by Fer-1 or DFO ($P < 0.05$). Conversely, the ferroptosis inducer erastin potentiated the cytotoxicity of both shikonin alone and the combination treatment (Figure 2A,B). This dependence on ferroptosis was further confirmed by colony formation assays, in which erastin suppressed and Fer-1 restored clonogenic survival (Figure 2C,D). Taken together, these findings indicate that the synergistic anti-proliferative effects of shikonin and osimertinib are primarily mediated through the induction of ferroptosis.

The shikonin-osimertinib combination triggers hallmarks of ferroptosis

Having established that ferroptosis mediates synergistic cell death, we next characterized the specific biochemical features of this process. The combination treatment significantly increased intracellular ROS (Figure 3A,B) and lipid ROS (Figure 3C,D) compared to monotherapies. Furthermore, MDA levels, indicative of lipid peroxidation, were markedly elevated in the combination group; this increase was further enhanced by erastin and rescued by Fer-1 (Figure 3E). GSH depletion was most pronounced in the combination group, an effect that was exacerbated by erastin and partially reversed by Fer-1 (Figure 3F). Finally, intracellular Fe^{2+} accumula-

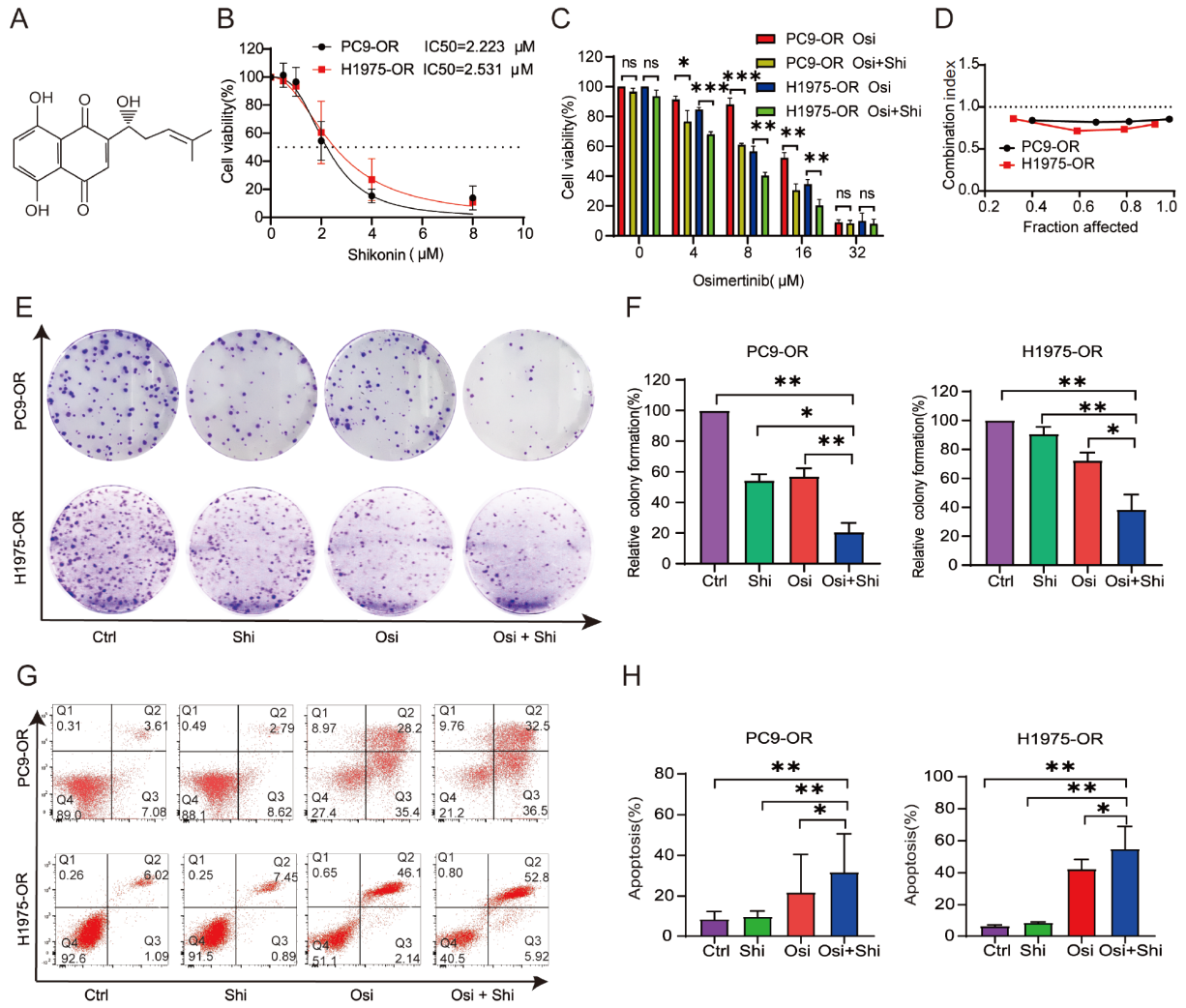


Figure 1. Shikonin enhances the cytotoxicity and antiproliferative effects of osimertinib in osimertinib-resistant LUAD cells (A) Chemical structure of shikonin. (B,C) Cells were treated with the specified concentrations of drugs for 48 h, and cell viability was assessed using the WST-1 assay. Representative experiment ($n = 5$ technical replicates; 3 independent experiments). (D) The synergistic effects of the combination treatment were evaluated by calculating CI values using Compusyn software, where CI < 1 indicates significant synergy. (E,F) Colony formation assays were conducted on cells treated with the drugs for 14 days. (G,H) Cells were exposed to the specified concentrations of drugs for 48 h, followed by analysis of apoptotic cells using Annexin V-FITC/PI staining. $n = 3$ technical replicates; 3 independent experiments. Ctrl, control; Shi, shikonin; Osi, osimertinib; Osi + Shi, combination of osimertinib and shikonin. Data are shown as the mean ± SD and were analyzed by a two-tailed unpaired Student's *t* test. ns, not significant. $^{*}P < 0.05$, $^{**}P < 0.01$, $^{***}P < 0.001$.

tion was also significantly enhanced by the drug combination (Figure 3G,H). Collectively, these findings demonstrate that shikonin potentiates the anti-tumor effects of osimertinib by robustly inducing the hallmark biochemical events of ferroptosis, ROS generation, lipid peroxidation, GSH depletion, and iron accumulation, in osimertinib-resistant LUAD cells.

HES1 downregulation mediates ferroptosis sensitization

To elucidate the molecular mechanisms underlying osimertinib resistance, we performed RNA-seq analysis of PC9-OR cells treated with various agents (Figure 4A). Differential expression analysis revealed that *HES1* mRNA was the most significantly downregulated transcript in the osimertinib and shikonin combination (Osi + Shi) treatment group compared to the control or either agent alone (Figure 4B,C). This central finding of *HES1* suppression by the synergistic combination was further corroborated by comparative transcriptome profiling of the parental PC9 and resistant PC9-OR cell lines (Figure 4D).

Given the central role of HES1 downregulation in our combination treatment, we next evaluated its clinical relevance. Analysis of TCGA data demonstrated that HES1 expression is elevated in LUAD tumor tissues compared to adjacent normal tissues (Supplementary Figure S2A,B). Moreover, high *HES1* expression correlated with poor patient prognosis (Supplementary Figure S2C) and showed diagnostic potential (AUC = 0.699; Supplementary Figure S2D). These bioinformatics observations were validated using our independent cohort of clinical specimens (Supplementary Figure S2E).

We then sought to confirm the functional role of HES1 at the cellular level. We first confirmed consistently higher HES1 expression in osimertinib-resistant cell lines (PC9-OR and H1975-OR) than in their sensitive counterparts (PC9 and H1975; Figure 4E). To

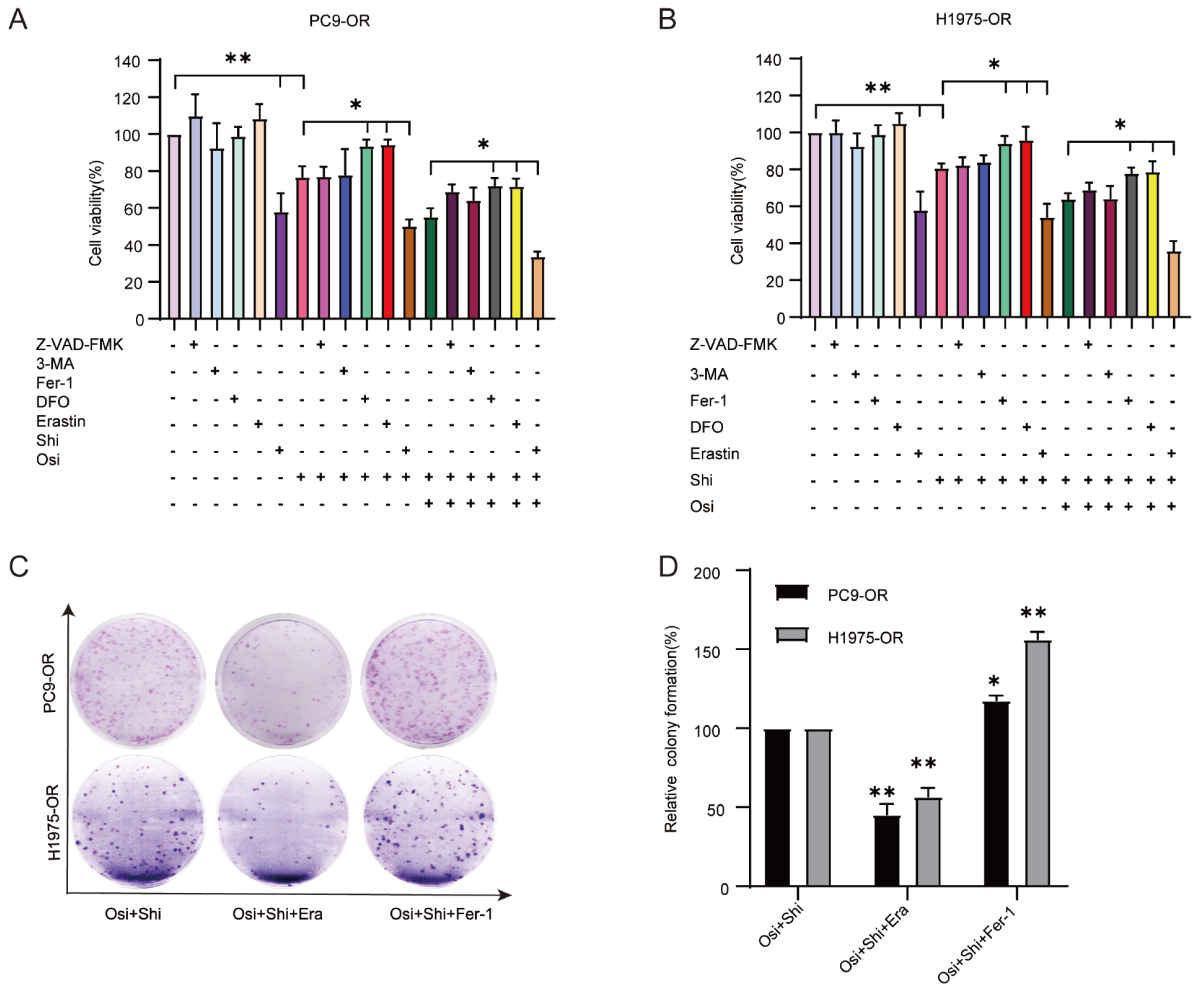


Figure 2. Shikonin synergizes with osimertinib to induce ferroptosis-dependent cell death in resistant LUAD cells (A,B) The impact of shikonin and osimertinib, along with other cell death inhibitors, on cell viability in PC9-OR and H1975-OR cells following 24 h of treatment. (C,D) Colony formation assays were performed on PC9-OR and H1975-OR cells treated with a combination of shikonin and osimertinib, with or without erastin or Fer-1, over 14 days. n = 3 technical replicates; 3 independent experiments. Ctrl, control; Shi, shikonin; Osi, osimertinib; Era, erastin; Fer-1, ferrostatin-1; DFO, deferoxamine. Data are shown as the mean ± SD and were analyzed by a two-tailed unpaired Student's t test. $^{*}P < 0.05$, $^{**}P < 0.01$.

assess its functional importance, we employed two distinct siRNAs and demonstrated that *HES1* knockdown significantly impaired cell viability (Figure 4F,G) and dramatically suppressed colony-forming capacity (Figure 4H,I) in resistant cells. Mechanistically, western blot analysis showed that *HES1* depletion led to the upregulation of ATF3 and concomitant downregulation of the ferroptosis regulator SLC7A11 (Figure 4J).

In summary, these findings position *HES1* as a key mediator of osimertinib resistance in LUAD. Its upregulation in clinical samples and resistant models, coupled with the profound phenotypic impact of its knockdown, suggests that HES1 serves as a critical target for the shikonin-osimertinib combination.

HES1 represses ATF3 to activate a ferroptosis defense program

To define the transcriptional network through which HES1 confers ferroptosis resistance, we performed an integrative bioinformatics analysis. Intersection of predicted target genes from multiple databases (GTRD, hTFtarget, Cistrome DB, and FerrDb V2) revealed ATF3 as a critical downstream target of HES1 (Figure 5A). Consistent with HES1 acting as a transcriptional repressor, ATF3 expression was significantly downregulated in LUAD tissues compared to adjacent normal tissues in TCGA datasets (Supplementary Figure S3A), a finding validated in our paired clinical samples (Supplementary Figure S3B). ROC analysis confirmed ATF3 as a robust diagnostic marker for LUAD (AUC = 0.815; Supplementary Figure S3C), and our clinical specimens exhibited concordantly reduced ATF3 mRNA levels in tumor tissues (Supplementary Figure S3D).

We next examined the expression and regulation of this HES1-ATF3 axis in our cellular models. In osimertinib-resistant LUAD cells (PC9-OR and H1975-OR), ATF3 mRNA and protein levels were markedly lower than those in their sensitive counterparts (PC9 and H1975). Conversely, the protein levels of HES1 and the key ferroptosis regulators SLC7A11 and GPX4 were elevated in resistant cells (Figure 5B,C). Notably, the combination therapy reversed these resistance-associated changes: ATF3 was upregulated, while HES1, SLC7A11, and GPX4 expressions were downregulated

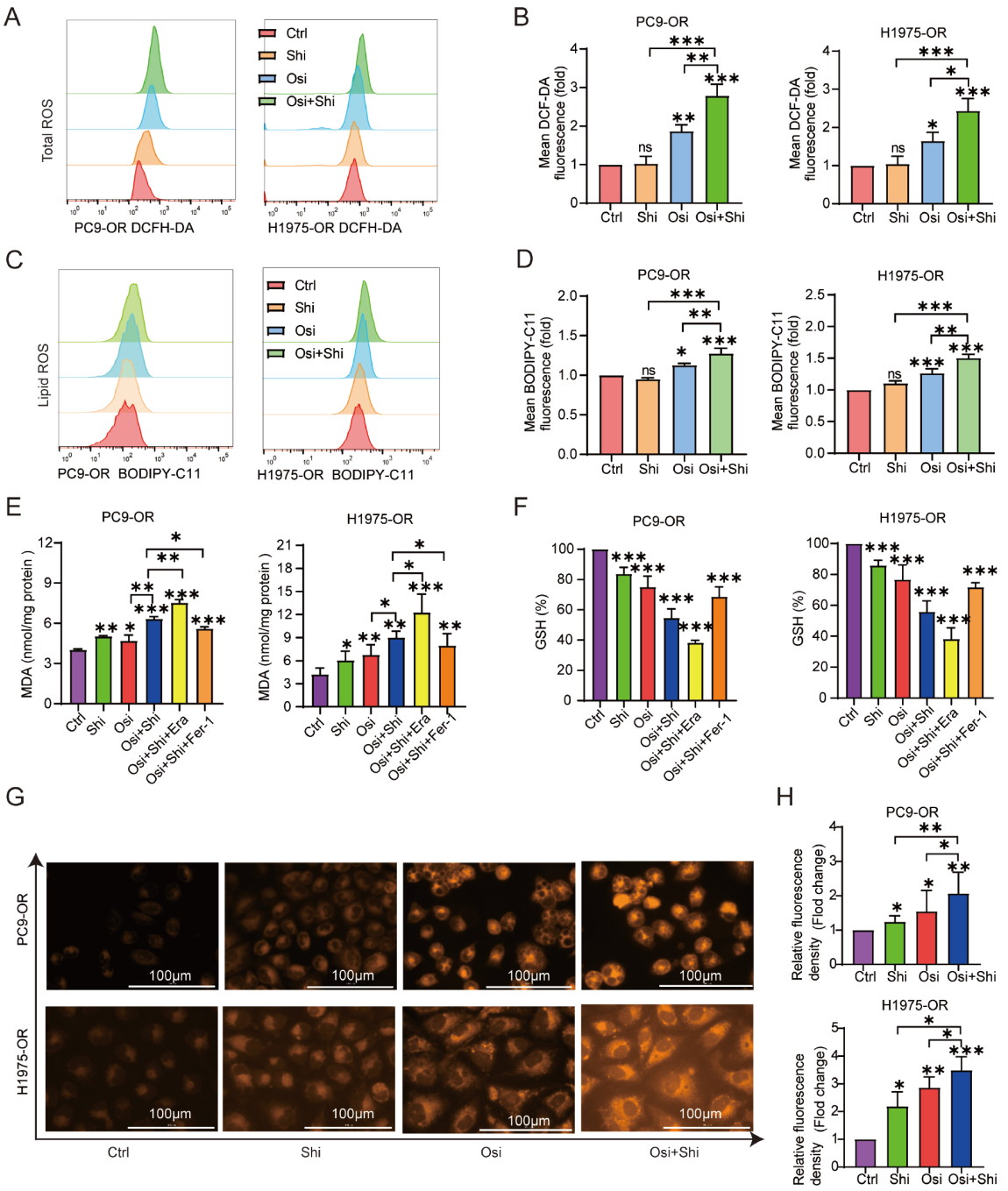


Figure 3. Shikonin synergizes with osimertinib to induce ferroptosis through ROS accumulation and iron dysregulation in resistant LUAD cells (A,B) Total ROS levels in PC9-OR and H1975-OR cells were assessed using a DCFH-DA fluorescence probe and analyzed by flow cytometry after 24 h of drug exposure. (C,D) Lipid peroxidation levels were measured in PC9-OR and H1975-OR cells using a C11-BODIPY 581/591 probe, followed by flow cytometry analysis after 24 h of treatment. (E) Intracellular MDA levels were measured in PC9-OR and H1975-OR cells after 24 h of drug treatment. (F) Relative GSH levels were assessed in PC9-OR and H1975-OR cells following 24 h of drug exposure. (G) FerroOrange staining was used to measure the levels of labile intracellular Fe^{2+} in PC9-OR and H1975-OR cells treated with drugs for 24 h. (H) Representative fluorescence intensity images from one of the five fields are shown, captured at identical exposure settings for each condition. Scale bar = 100 μm. Ctrl, control; Shi, shikonin; Osi, osimertinib; Era, erastin; Fer-1, ferrostatin-1. $n = 3$ technical replicates; 3 independent experiments. Data are shown as the mean ± SD and were analyzed by a two-tailed unpaired Student's t test. ns, not significant. $^*P < 0.05$, $^{**}P < 0.01$, $^{***}P < 0.001$.

(Figure 5D). The addition of erastin intensified these expression shifts, whereas Fer-1 reversed them (Figure 5E), strongly supporting the functional involvement of ferroptosis in this regulatory axis.

To establish a direct causal link, we genetically modulated HES1. Knockdown of *HES1* in resistant cells (PC9-OR and H1975-OR) significantly suppressed *HES1* mRNA level, increased *ATF3* mRNA level and decreased *SLC7A11* and *GPX4* mRNA levels (Supplementary Figure S4A–H), suggesting that HES1 negatively regulates ATF3 but positively modulates SLC7A11 and GPX4. This specific repressive relationship between HES1 and ATF3 was further

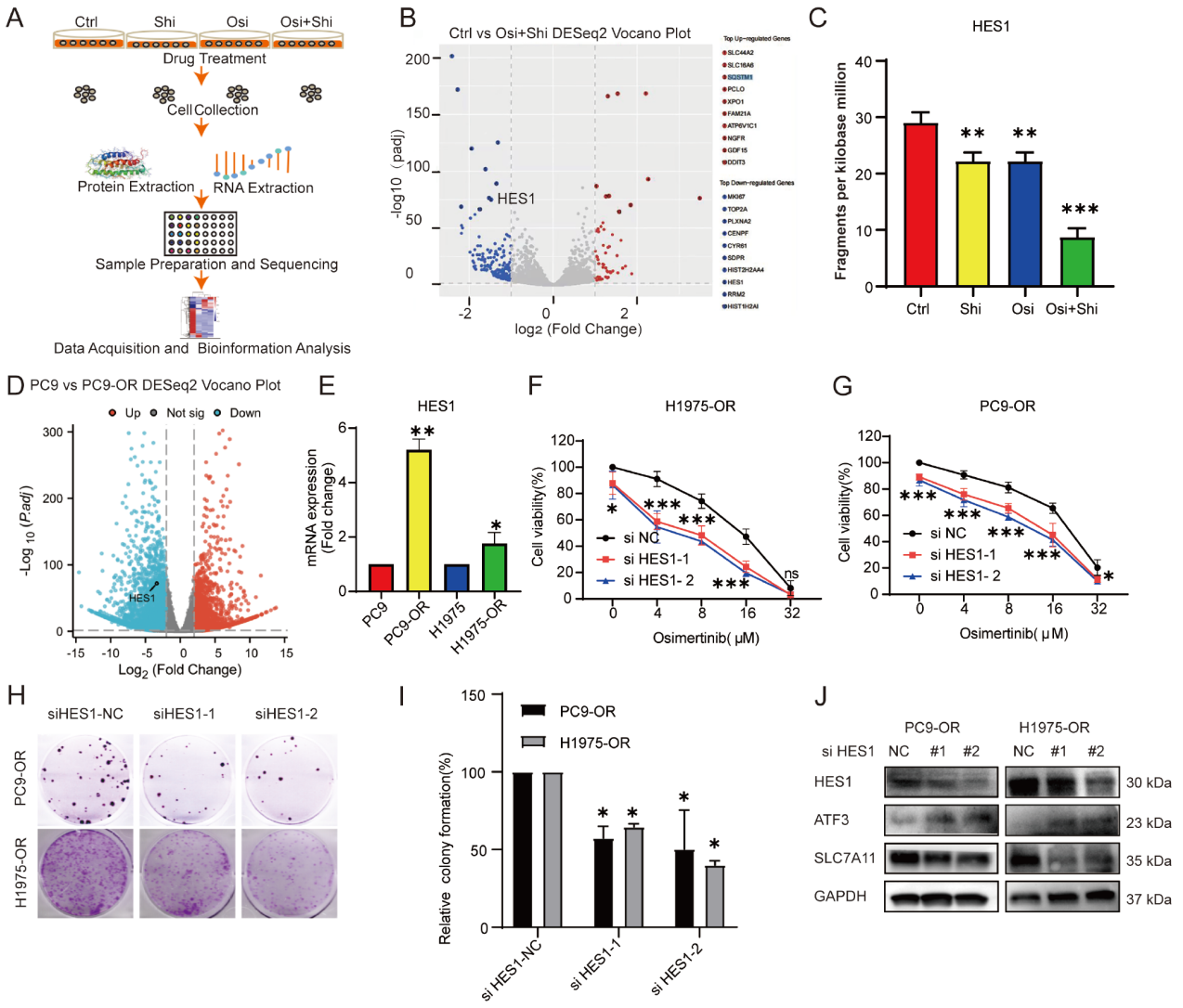


Figure 4. Integrated multiomics analysis reveals HES1-mediated ferroptosis resistance in osimertinib-resistant LUAD cells (A) Workflow for proteomic and genomic analyses of the combination treatment. (B) Volcano plot illustrating differentially expressed mRNAs between the control and osimertinib + shikonin groups in PC9-OR cells. (C) RNA-seq results for HES1 in PC9-OR cells treated with the indicated concentrations of drugs for 48 h. (D) Volcano plot illustrating differentially expressed mRNAs between PC9 and PC9-OR cells. (E) Relative RNA expression levels of *HES1* in osimertinib-sensitive and osimertinib-resistant LUAD cells were measured via qRT-PCR. (F,G) PC9-OR and H1975-OR cells were treated with specified concentrations of osimertinib for 24 h, with or without *HES1* knockdown, followed by cell viability assays. Cell viability data were normalized to the 0 μM osimertinib control for each respective siRNA group (siNC, siHES1-1, or siHES1-2). (H) Colony formation assay of PC9-OR and H1975-OR cells with or without *HES1* knockdown for 14 days. (I) Quantification of colony formation in PC9-OR and H1975-OR cells from panel G. (J) HES1, ATF3, and SLC7A11 protein levels in PC9-OR and H1975-OR cells with or without *HES1* knockdown for 48 h. Ctrl, control; Shi, shikonin; Osi, osimertinib. n = 3 technical replicates; 3 independent experiments. Data are shown as the mean ± SD and were analyzed by a two-tailed unpaired Student's t test. ns: not significant. $^{*}P < 0.05$, $^{**}P < 0.01$, $^{***}P < 0.001$.

confirmed in 293T cells, where HES1 overexpression reduced ATF3 expression, while *HES1* knockdown increased it (Figure 5F).

HES1 transcriptionally represses ATF3 to inhibit ferroptosis

To further elucidate the transcriptional regulatory mechanisms of HES1, we investigated whether it directly modulates ATF3, SLC7A11 or GPX4 expression. ChIP assays demonstrated specific binding of HES1 to the *ATF3* promoter region in PC9-OR cells (Figure 6A,B), with anti-HES1 antibody showing significantly higher enrichment than the IgG control. Importantly, no significant HES1 binding was detected at the *SLC7A11* or *GPX4* promoter (Supplementary Figure S5A,B), indicating that HES1 does not directly regulate these genes. Complementary dual-luciferase reporter assays in 293T cells revealed that HES1 overexpression (OE-HES1) substantially attenuated *ATF3* promoter-driven luciferase activity (Figure 6C), supporting HES1's repressive effect on ATF3 transcription.

To pinpoint the precise binding site, we performed a comprehensive bioinformatics analysis using the JASPAR database, which identified two potential HES1-binding sites within the *ATF3* promoter region (Figure 6D,E). Functional characterization demonstrated that mutation of site-1 (5′-CACGCTCT-3′, –910 to –903 nt) had minimal effect, whereas mutation of site-2 (5′-TGCGTGTG-3′,

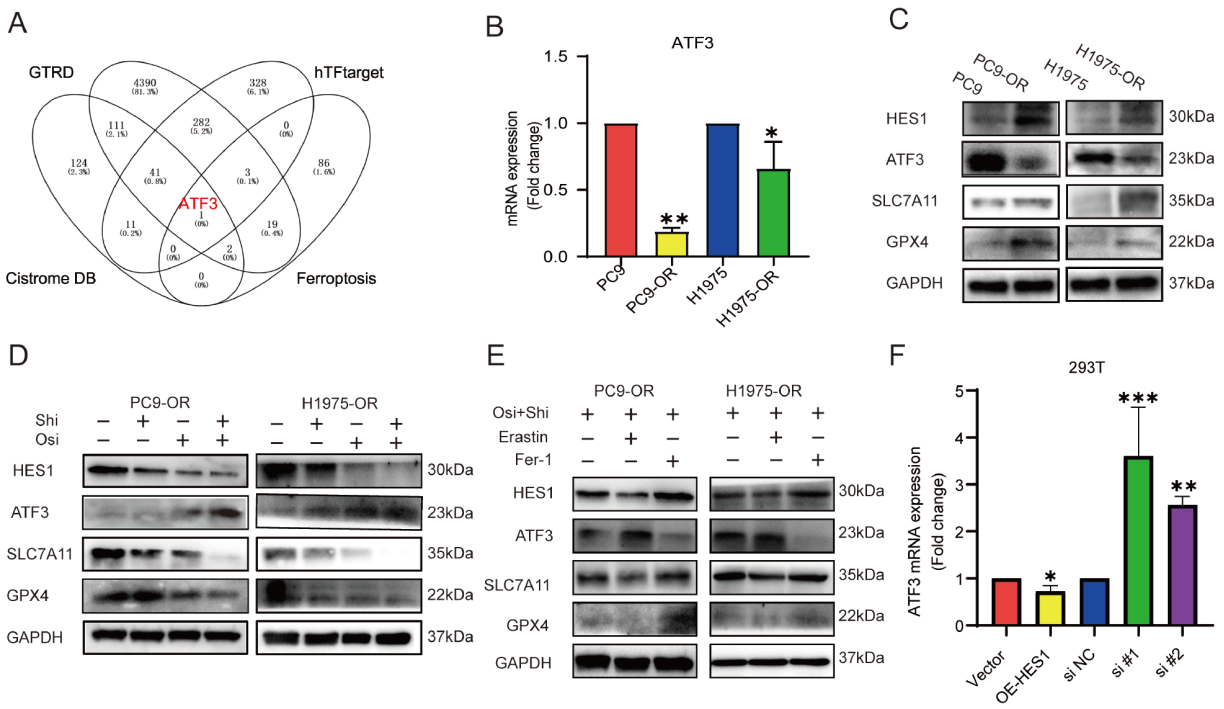


Figure 5. HES1 regulates ferroptosis-related genes in osimertinib-resistant LUAD cells (A) Venn diagram showing the overlap of *HES1* target genes and ferroptosis-related genes across multiple datasets. (B) Relative *ATF3* mRNA expression in osimertinib-sensitive and osimertinib-resistant LUAD cells. (C) Protein levels of HES1, ATF3, SLC7A11, and GPX4 in osimertinib-sensitive and osimertinib-resistant LUAD cells. (D) Western blot analysis of HES1 and ferroptosis-related proteins (ATF3, SLC7A11, and GPX4) in cells treated with or without drugs for 48 h. (E) Expressions of HES1 and ferroptosis-related proteins (ATF3, SLC7A11, and GPX4) in cells treated with the combination treatment with or without erastin or Fer-1 for 48 h. (F) *ATF3* mRNA expression in 293T cells with HES1 overexpression or knockdown, as assessed by qRT-PCR. $n = 3$ technical replicates; 3 independent experiments. Data are shown as the mean ± SD and were analyzed by a two-tailed unpaired Student's *t* test. $^{*}P < 0.05$, $^{**}P < 0.01$, $^{***}P < 0.001$.

−786 to −779 nt) significantly abrogated HES1-mediated transcriptional repression (Figure 6F). These results define a specific mechanism wherein HES1 negatively regulates *ATF3* transcription by binding primarily to the site-2 region of its promoter.

We then sought to determine whether ATF3 is the primary functional effector downstream of HES1. We performed a rescue experiment by knocking down *ATF3* in siHES1 osimertinib-resistant cells. Consistent with its repressive role, *HES1* knockdown led to a significant upregulation of ATF3 expression (Supplementary Figure S6A,B). Subsequent introduction of ATF3-specific siRNA effectively reduced *ATF3* mRNA levels (Supplementary Figure S6B). Strikingly, *ATF3* depletion largely reversed the suppression of SLC7A11 (Supplementary Figure S6C) and GPX4 (Supplementary Figure S6D) expressions caused by *HES1* knockdown. This genetic rescue experiment demonstrates that the induction of ferroptosis defense genes following *HES1* loss is critically dependent on ATF3 derepression, providing compelling evidence that ATF3 is the key downstream mediator through which HES1 orchestrates ferroptosis resistance in LUAD.

The osimertinib-shikonin combination inhibits tumor growth *in vivo* via the HES1/ATF3 axis without systemic toxicity

We next evaluated the therapeutic efficacy and safety of the combination treatment in a mouse xenograft model. The combination of osimertinib and shikonin significantly suppressed tumor growth and reduced final tumor size compared to the control group or either monotherapy (Figure 7A–D). Importantly, the treatment did not elicit observable toxic effects, as evidenced by stable body weights throughout the study (Figure 7E) and the absence of significant changes in serum markers of hepatic (ALT and AST) and renal (BUN and CRE) function, as well as total protein (TP) and albumin (ALB) levels (Figure 7F–K).

Histological analysis of tumor tissues provided further mechanistic insights. H&E staining revealed that the combination treatment caused the most pronounced tissue damage, characterized by reduced cell density and nuclear distortion (Figure 7L–P). Consistent with our *in vitro* findings, immunohistochemical staining demonstrated that the combination treatment significantly downregulated the proliferation marker Ki-67 and the protein levels of HES1 and SLC7A11 while markedly upregulating ATF3 expression compared to all other groups (Figure 7L–P and Supplementary Figure S7).

Collectively, these *in vivo* results demonstrate that the shikonin-osimertinib combination effectively inhibits tumor growth without systemic toxicity and enhances antitumor efficacy by modulating the HES1/ATF3 axis, thereby inducing ferroptosis.

Discussion

Osimertinib, a third-generation EGFR-TKI, is the preferred initial treatment for individuals with advanced LUAD with EGFR mutations [32]. However, its long-term efficacy is frequently compromised by the emergence of acquired resistance, representing a major clinical challenge in NSCLC management. Recent studies

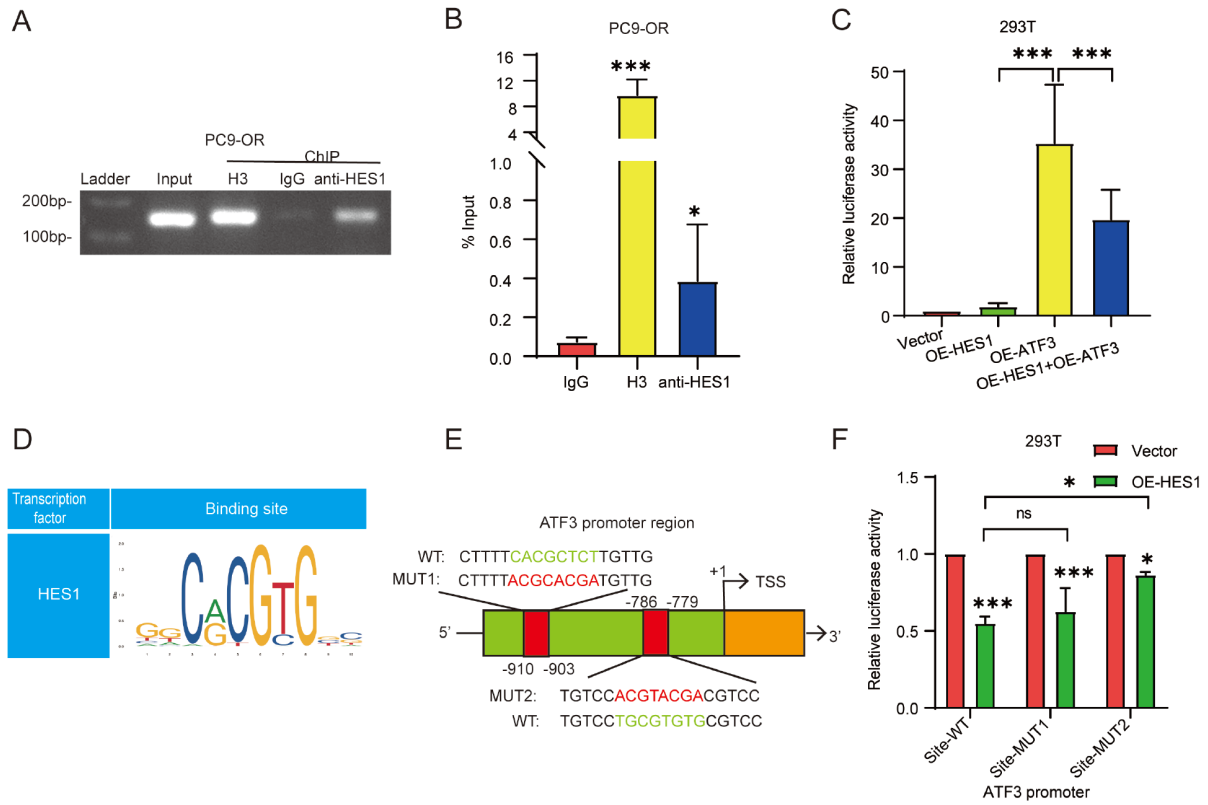


Figure 6. Shikonin combined with osimertinib induces ferroptosis by downregulating HES1, which binds to and negatively regulates *ATF3* transcription in LUAD cells (A,B) ChIP-qRT-PCR analysis of HES1 binding to the *ATF3* promoter in PC9-OR cells and agarose gel electrophoresis. (C) Dual-luciferase reporter assays were used to measure the *ATF3* promoter activity in 293T cells, with luciferase activity normalized to *Renilla* luciferase activity. The input served as a positive control, whereas IgG was used as a negative control. (D) Predicted HES1-binding sites in the *ATF3* promoter region identified using the JASPAR database. (E) Schematic representation of predicted HES1-binding sites in the 5′ region of *ATF3*: Mut1 (–910 to –903 nt) and Mut2 (–786 to –779 nt). (K) Wild-type (WT) or mutant (Mut) *ATF3* luciferase reporter vectors were co-transfected with either HES1 or a control vector into 293T cells, and luciferase activity was measured. $n = 3$ technical replicates; 3 independent experiments. Data are shown as the mean ± SD and were analyzed by a two-tailed unpaired Student's t test. ns, not significant. $^{*}P < 0.05$, $^{***}P < 0.001$.

have investigated various strategies to overcome osimertinib resistance in LUAD [33,34], including targeted therapy, platinum-based chemotherapy, immunotherapy, and TCM. Among these, TCM has gained attention for its potential to enhance the efficacy of targeted therapies. Several herbal compounds in TCM have shown promise in reversing drug resistance [35,36], improving patient quality of life, and mitigating the side effects associated with osimertinib [37]. These findings suggest that integrating TCM with osimertinib could be a promising strategy for reducing or reversing resistance.

Shikonin has shown potential as an anticancer therapy for various types of cancer, including colon, breast, prostate, ovarian, cervical, glioblastoma, and lung cancers [38,39]. However, the antitumor effects and mechanisms of the combination of shikonin and osimertinib in osimertinib-resistant LUAD remain unclear. In this study, we found that shikonin combined with osimertinib synergistically suppressed proliferation and colony formation in osimertinib-resistant LUAD cells, as evidenced by the combination index analysis. The combination treatment increased total ROS, lipid ROS, MDA, and intracellular Fe^{2+} accumulation while significantly decreasing GSH levels in resistant LUAD cells. These results suggest that the combination was more effective at inducing ferroptosis, a regulated form of cell death marked by iron-dependent lipid peroxidation, than either drug alone. Notably, ferroptosis induction was reversible by Fer-1 and enhanced by erastin, confirming that this combination overcomes resistance primarily through the ferroptosis pathway. These results align with emerging research highlighting the role of ferroptosis in cancer therapy, particularly in overcoming drug resistance.

To corroborate the biochemical evidence of ferroptosis at the molecular level, we next assessed the expressions of its key regulators. Central to ferroptosis regulation are SLC7A11 and GPX4, whose downregulation is widely regarded as a hallmark of ferroptotic activity [19]. Inhibition of these proteins to promote ferroptosis has emerged as a promising antitumor strategy. For instance, Wang *et al.* [40] demonstrated that TRIM3 suppresses NSCLC tumorigenesis by degrading SLC7A11 and thereby inducing ferroptosis. Another study reported that CTRP6 promotes lung cancer progression by stabilizing SOCS2 and enhancing the xCT/GPX4 axis, thereby attenuating ferroptosis [41]. These prior studies highlight the therapeutic potential of targeting SLC7A11/GPX4, yet the transcriptional landscape controlling this axis in osimertinib-resistant LUAD is poorly defined. This gap prompted our investigation, which ultimately identified HES1/ATF3 as a key transcriptional switch.

Indeed, exploiting ferroptosis represents a promising strategy to overcome the canonical resistance mechanisms, such as enhanced drug efflux, target alteration, and apoptosis evasion, which plague

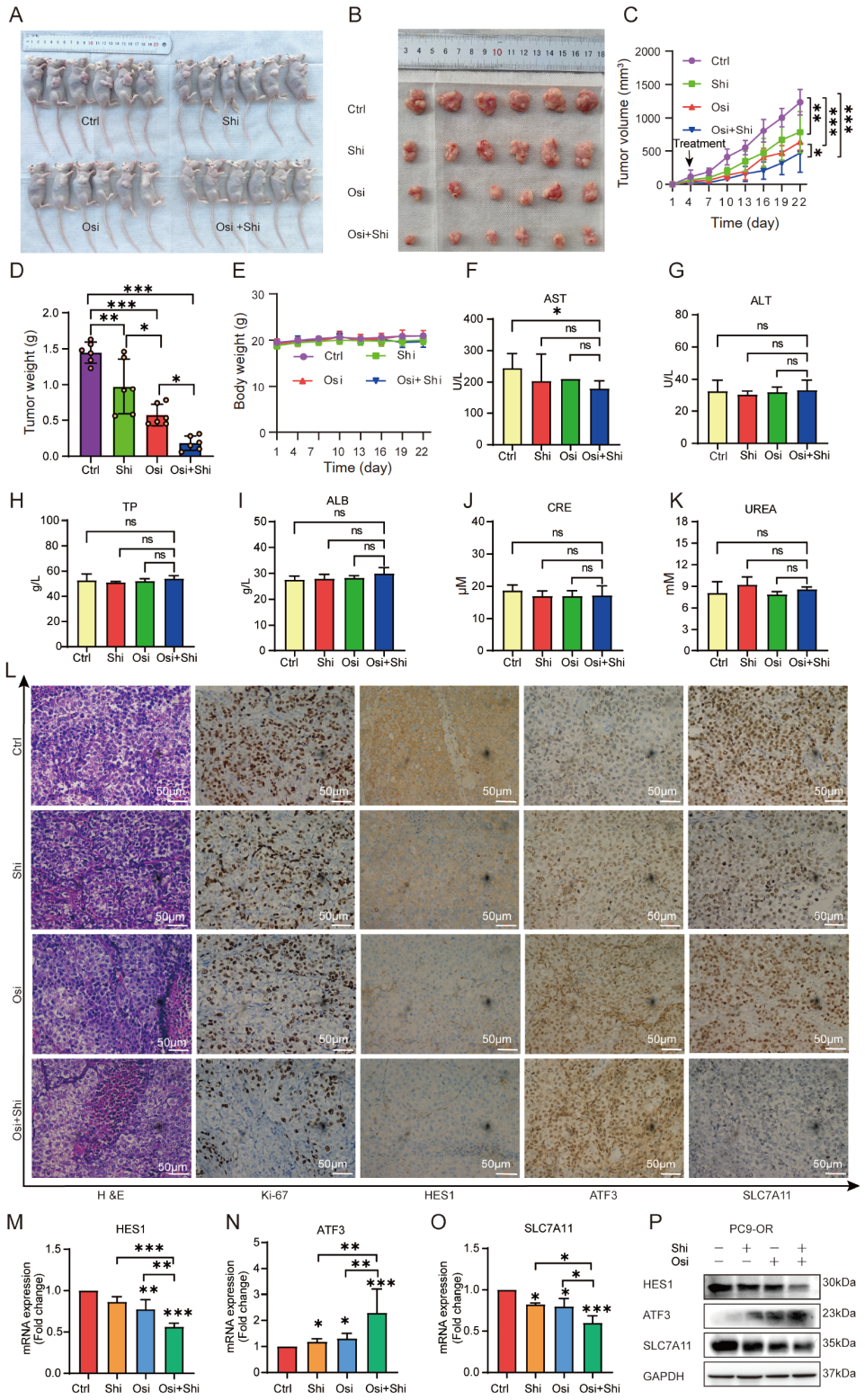


Figure 7. The combination treatment of osimertinib and shikonin synergistically inhibits tumor growth *in vivo* without causing significant toxicity (A) Photographic documentation of tumor-bearing mice subjected to various treatments. (B) Representative images of xenografted tumors in mice after 22 days of treatment with or without drugs. (C) Changes in the tumor volume in mice during different treatment regimens. (D) Tumor weight measurement after the treatment period. (E) Changes in body weight during the various treatment protocols. (F–K) ALT (F), AST (G), TP (H), ALB (I), CRE (J), and UREA (K) in mice after 22 days of treatment. (L) H&E staining and immunohistochemical (IHC) analysis of the xenografted tumor tissues. Scale bar = 50 μm. (M–O) Quantitative PCR analysis of *HES1*, *ATF3*, and *SLC7A11* mRNA expressions in xenograft tumor tissues. (P) Western blot analysis of HES1, ATF3, and SLC7A11 protein expressions in xenograft tumor tissues (n = 6 mice per group). Ctrl, control; Shi, shikonin; Osi, osimertinib. ns, not significant. $^{*}P < 0.05$, $^{**}P < 0.01$, $^{***}P < 0.001$.

conventional therapies. By targeting iron homeostasis and lipid peroxidation, ferroptosis can circumvent these barriers to eliminate drug-resistant cancer cells. Studies have shown that NSCLC cells that are resistant to EGFR inhibitors can be sensitized to ferroptosis. For instance, vorinostat triggers ferroptosis by downregulating SLC7A11 [25], while dauricine acts through SAT1 stabilization [23]. Similarly, Wang *et al.* [42] reported that a nanocatalytic sensitizer combined with AHP-DRI-12 overcomes AZD9291 resistance via ferroptosis induction. Consistently, our study establishes that the shikonin-osimertinib combination effectively induces ferroptosis in resistant LUAD cells. We observed a characteristic decrease in the key ferroptosis regulators SLC7A11 and GPX4, concomitant with the upregulation of ATF3. Crucially, this ferroptotic cell death was reversible by ferrostatin-1 and enhanced by erastin, confirming the specificity of the mechanism involved.

To identify key molecular determinants of ferroptosis sensitivity, we focused on transcriptional regulators that might orchestrate this process. Among the candidates, the transcriptional repressor HES1 emerged as a prime target due to its established role in therapy resistance. HES1 serves as a critical transcriptional repressor involved in essential biological functions such as cell differentiation, cycle regulation, apoptosis, and self-renewal [43]. Clinically, elevated HES1 expression correlates with poor prognosis in LUAD [44] and increases during relapse in EGFR-TKI-treated patients [45]. Beyond LUAD, HES1 contributes to multidrug resistance in other malignancies: in colorectal cancer, elevated HES1 promotes chemotherapy resistance through EMT induction and ABC transporter activation [46]. Notably, HES1 downregulation sensitizes LUAD to EGFR-TKIs. Zhang *et al.* [47] reported that the NOTCH4$^{\Delta L12_16}$ mutation enhances EGFR-TKI sensitivity via HES1 downregulation, while Bousquet *et al.* [45] and Takahashi *et al.* [30] showed that Notch pathway inhibition overcomes osimertinib resistance by reducing HES1 levels. Consistently, our results showed that the shikonin-osimertinib combination suppressed HES1 expression, an effect reversible by Fer-1, underscoring the importance of HES1 inhibition in overcoming osimertinib resistance. It is worth noting that the tumor microenvironment plays a crucial role in therapy resistance. Recent studies have shown that cancer-associated fibroblasts promote tumor progression and immunosuppression in LUAD through PDGFC secretion [48], suggesting that future studies should explore potential crosstalk between TME components and HES1-mediated resistance mechanisms.

Having established HES1 as a critical node in osimertinib resistance, we next sought to delineate the precise molecular mechanisms through which it regulates ferroptosis. Our data support a model wherein HES1 drives resistance by suppressing ATF3 expression, thereby activating the SLC7A11/GPX4-mediated ferroptosis defense pathway. Specifically, we provide evidence that HES1 directly binds to the *ATF3* promoter to repress its transcription, a novel mechanism that enhances ferroptosis resistance in LUAD and underlies osimertinib treatment failure.

Previous studies have shown that erastin can upregulate ATF3, which binds to the *SLC7A11* promoter, represses its transcription, and promotes ferroptosis [49]. Additionally, ATF3 has been reported to facilitate ferroptosis in glioblastoma cells by suppressing *SLC7A11* transcription [50]. It has been reported that shikonin suppresses SCLC by inducing ferroptosis that is dependent on ATF3 [31]. Our study also revealed that the combination treatment upregulated ATF3 and downregulated SLC7A11 and GPX4, facilitating ferroptosis. Thus, our work provides evidence that the combination of shikonin and osimertinib overcomes osimertinib resistance by inducing ferroptosis, potentially through the HES1/ATF3 axis.

While our findings delineate a novel role for the HES1/ATF3 axis in overcoming osimertinib resistance, several limitations of this study should be acknowledged. First, our *in vitro* models may not fully recapitulate the influence of the TME on ferroptosis sensitivity. Second, the translational potential of targeting HES1 requires validation using preclinical models. Third, our mechanistic studies demonstrating the direct binding of HES1 to the *ATF3* promoter and subsequent transcriptional repression were conducted in 293T cells. Future work should aim to confirm this regulatory interaction directly in osimertinib-resistant LUAD models, which may possess a distinct transcriptional landscape. Fourth, key rescue experiments, including *ATF3* knockdown and SLC7A11 overexpression/cystine supplementation in LUAD-OR cells, are needed to definitively establish causal relationships in the proposed pathway. Finally, the therapeutic efficacy of *HES1* knockdown should be explored in future *in vivo* studies.

In summary, shikonin synergistically enhances the antiproliferative effects of osimertinib in osimertinib-resistant LUAD cells. The underlying mechanism involves shikonin-induced ferroptosis via HES1-mediated ATF3 upregulation, offering a promising strategy to overcome osimertinib resistance in LUAD.

Supplementary Data

Supplementary data are available at *Acta Biochimica et Biophysica Sinica* online.

Data Availability

The sequence data reported in this paper have been deposited in the OMIX, China National Center for Bioinformation/Beijing Institute of Genomics, Chinese Academy of Sciences (https://ngdc.cncb.ac.cn/omix; accession No. OMIX014581 and no. OMIX014620). All other data supporting the findings of this study are available from the corresponding author upon reasonable request.

Author contributions

H.W.L., Q.Y., and L.Y.: investigation, data curation, formal analysis, and writing of the original draft. X.B.H., Y.Y.C., Y.H.C, Y.X.Z, X.L., and M.Y.: investigation, data curation. Y.T.J., Y.D.G., Y.F.L., Q.H.L., and Z.X.Y.: visualization, methodology, software. W.M.S. and L.L.Y.: supervision, validation, funding acquisition, writing, review, and editing.

Funding

This work was supported in part by the grants from the National Natural Science Foundation of China (No. 82073388 to S.W.M.), the Natural Outstanding Youth Fund of Guangdong Province (No. 2022B1515020090 to S.W.M.), Guangdong Provincial Key Laboratory of Autophagy and Major Chronic Non-communicable Diseases (No. 2022B1212030003 to S.W.M.), Affiliated Hospital of Guangdong Medical University Clinical Research Program (Nos. LCYJ2020B005 and LCY2022DL002 to S.W.M.), Zhanjiang Key Laboratory of Tumor Microenvironment and Organoid Research (to S.W.M.), and the Beijing Kechuang Medical Development

Foundation (No. KC2023-JX-0288-PM30 to S.W.M.).

Conflict of Interest

The authors declare that they have no conflict of interest.

References

1. Bray F, Laversanne M, Sung H, Ferlay J, Siegel RL, Soerjomataram I, Jemal A. Global cancer statistics 2022: GLOBOCAN estimates of incidence and mortality worldwide for 36 cancers in 185 countries. *CA Cancer J Clin* 2024, 74: 229–263
2. Hendriks LEL, Remon J, Faivre-Finn C, Garassino MC, Heymach JV, Kerr KM, Tan DSW, *et al.* Non-small-cell lung cancer. *Nat Rev Dis Primers* 2024, 10: 71
3. Riely GJ, Wood DE, Ettinger DS, Aisner DL, Akerley W, Bauman JR, Bharat A, *et al.* Non-small cell lung cancer, version 4.2024. *J Natl Compr Cancer Netw* 2024, 22: 249–274
4. Planchard D, Jänne PA, Cheng Y, Yang JCH, Yanagitani N, Kim SW, Sugawara S, *et al.* Osimertinib with or without chemotherapy in *EGFR*-mutated advanced NSCLC. *N Engl J Med* 2023, 389: 1935–1948
5. Ramalingam SS, Vansteenkiste J, Planchard D, Cho BC, Gray JE, Ohe Y, Zhou C, *et al.* Overall survival with osimertinib in untreated, *EGFR*-mutated advanced NSCLC. *N Engl J Med* 2020, 382: 41–50
6. Tsuboi M, Herbst RS, John T, Kato T, Majem M, Grohé C, Wang J, *et al.* Overall survival with osimertinib in resected *EGFR*-mutated NSCLC. *N Engl J Med* 2023, 389: 137–147
7. Sequist LV, Han JY, Ahn MJ, Cho BC, Yu H, Kim SW, Yang JCH, *et al.* Osimertinib plus savolitinib in patients with EGFR mutation-positive, MET-amplified, non-small-cell lung cancer after progression on EGFR tyrosine kinase inhibitors: interim results from a multicentre, open-label, phase 1b study. *Lancet Oncol* 2020, 21: 373–386
8. Lu C, Zhang Z, Fan Y, Wang X, Qian J, Bian Z. Shikonin induces ferroptosis in osteosarcomas through the mitochondrial ROS-regulated HIF-1α/HO-1 axis. *Phytomedicine* 2024, 135: 156139
9. Markowitsch SD, Vakhrusheva O, Schupp P, Akele Y, Kitanovic J, Slade KS, Efferth T, *et al.* Shikonin inhibits cell growth of sunitinib-resistant renal cell carcinoma by activating the necrosome complex and inhibiting the AKT/mTOR signaling pathway. *Cancers* 2022, 14: 1114
10. Zhang N, Peng F, Wang Y, Yang L, Wu F, Wang X, Ye C, *et al.* Shikonin induces colorectal carcinoma cells apoptosis and autophagy by targeting galectin-1/JNK signaling axis. *Int J Biol Sci* 2020, 16: 147–161
11. Lew CY, Tang YT, Lee AYJ, Chin ZJ, Chang WL, Chen CH, Chye SM. Shikonin as a dietary phytochemical with multi-target anti-cancer activities: from molecular mechanisms to translational applications. *Nutrients* 2025, 17: 3085
12. Yen JH, Keak PY, Wu CL, Chen HJ, Gao WY, Liou JW, Chen YR, *et al.* Shikonin, a natural naphthoquinone phytochemical, exerts anti-leukemia effects in human CBF-AML cell lines and zebrafish xenograft models. *Biomed Pharmacother* 2024, 179: 117395
13. Doddapaneni R, Tucker JD, Lu PJ, Lu QL. Synergistic effect of ribitol and shikonin promotes apoptosis in breast cancer cells. *Int J Mol Sci* 2025, 26: 2661
14. Markowitsch SD, Juetter KM, Schupp P, Hauschulte K, Vakhrusheva O, Slade KS, Thomas A, *et al.* Shikonin reduces growth of docetaxel-resistant prostate cancer cells mainly through necroptosis. *Cancers* 2021, 13: 882
15. Ni M, Zhou J, Zhu Z, Xu Q, Yin Z, Wang Y, Zheng Z, *et al.* Shikonin and cisplatin synergistically overcome cisplatin resistance of ovarian cancer by inducing ferroptosis via upregulation of HMOX1 to promote Fe^{2+} accumulation. *Phytomedicine* 2023, 112: 154701
16. Hu X, Peng X, Zhang Y, Fan S, Liu X, Song Y, Ren S, *et al.* Shikonin reverses cancer-associated fibroblast-induced gemcitabine resistance in pancreatic cancer cells by suppressing monocarboxylate transporter 4-mediated reverse Warburg effect. *Phytomedicine* 2024, 123: 155214
17. Wang L, Stadlbauer B, Lyu C, Buchner A, Pohla H. Shikonin enhances the antitumor effect of cabazitaxel in prostate cancer stem cells and reverses cabazitaxel resistance by inhibiting ABCG2 and ALDH3A1. *Am J Cancer Res* 2020, 10: 3784–3800
18. Deng H, Zhang H, Zhao Y, Chen T, Mao X, Li J, Li M, *et al.* Co-encapsulated with shikonin/doxorubicin pH-sensitive liposomes: preparation, characterization and its synergistic effect in drug-resistant breast cancer cells. *J Pharm Sci* 2025, 114: 103974
19. Stockwell BR. Ferroptosis turns 10: emerging mechanisms, physiological functions, and therapeutic applications. *Cell* 2022, 185: 2401–2421
20. Xu G, Liang Q, Gao L, Xu S, Luo W, Wu Q, Li J, *et al.* Developing an arene binuclear ruthenium(II) complex to induce ferroptosis and activate the cGAS-STING pathway: targeted inhibiting growth and metastasis of triple negative breast cancer. *J Med Chem* 2024, 67: 19573–19585
21. Zhao L, Zhou X, Xie F, Zhang L, Yan H, Huang J, Zhang C, *et al.* Ferroptosis in cancer and cancer immunotherapy. *Cancer Commun* 2022, 42: 88–116
22. Zhang C, Liu X, Jin S, Chen Y, Guo R. Ferroptosis in cancer therapy: a novel approach to reversing drug resistance. *Mol Cancer* 2022, 21: 47
23. Men B, Chen Z, Ge H, Yang Z, Yun L, Jiang J, Dian M, *et al.* Dauricine overcomes osimertinib resistance in lung cancer by inducing ferroptosis via stabilizing SAT1. *Cancer Sci* 2025, 116: 2256–2269
24. Fu D, Wang C, Yu L, Yu R. Induction of ferroptosis by ATF3 elevation alleviates cisplatin resistance in gastric cancer by restraining Nrf2/Keap1/xCT signaling. *Cell Mol Biol Lett* 2021, 26: 26
25. Zhang T, Sun B, Zhong C, Xu K, Wang Z, Hofman P, Nagano T, *et al.* Targeting histone deacetylase enhances the therapeutic effect of erastin-induced ferroptosis in EGFR-activating mutant lung adenocarcinoma. *Transl Lung Cancer Res* 2021, 10: 1857–1872
26. Magesh V, Sekar R, AlZahrani A, Balasubramanian R, Abdelsalam SA, Rajendran P. HES1 in cancer: a key player in tumorigenesis and its prognostic significance. *Mol Genet Genomics* 2025, 300: 49
27. Chmielecki J, Foo J, Oxnard GR, Hutchinson K, Ohashi K, Somwar R, Wang L, *et al.* Optimization of dosing for EGFR-mutant non-small cell lung cancer with evolutionary cancer modeling. *Sci Transl Med* 2011, 3: 90ra59
28. Xia L, Yang F, Wu X, Li S, Kan C, Zheng H, Wang S. SHP2 inhibition enhances the anticancer effect of Osimertinib in EGFR T790M mutant lung adenocarcinoma by blocking CXCL8 loop mediated stemness. *Cancer Cell Int* 2021, 21: 337
29. Kleczko EK, Le AT, Hinz TK, Nguyen TT, Navarro A, Hu CJ, Selman AM, *et al.* Novel EGFR-mutant mouse models of lung adenocarcinoma reveal adaptive immunity requirement for durable osimertinib response. *Cancer Lett* 2023, 556: 216062
30. Takahashi H, Sakakibara-Konishi J, Furuta M, Shoji T, Tsuji K, Morinaga D, Kikuchi E, *et al.* Notch pathway regulates osimertinib drug-tolerant persistence in *EGFR*-mutated non-small-cell lung cancer. *Cancer Sci* 2023, 114: 1635–1650
31. Qian X, Zhu L, Xu M, Liu H, Yu X, Shao Q, Qin J. Shikonin suppresses small cell lung cancer growth via inducing ATF3-mediated ferroptosis to promote ROS accumulation. *Chem-Biol Interact* 2023, 382: 110588
32. Ramalingam SS, Yang JCH, Lee CK, Kurata T, Kim DW, John T, Nogami N, *et al.* Osimertinib as first-line treatment of *EGFR* mutation-positive advanced non–small-cell lung cancer. *J Clin Oncol* 2018, 36: 841–849
33. Fu K, Xie F, Wang F, Fu L. Therapeutic strategies for EGFR-mutated non-small cell lung cancer patients with osimertinib resistance. *J Hematol*

Oncol 2022, 15: 173

34. Chen L, Chen WD, Xu YX, Ren YY, Zheng C, Lin YY, Zhou JL. Strategies for enhancing non-small cell lung cancer treatment: integrating Chinese herbal medicines with epidermal growth factor receptor-tyrosine kinase inhibitors therapy. *Eur J Pharmacol* 2024, 980: 176871
35. Huang G, Liu X, Jiang T, Cao Y, Sang M, Song X, Zhou B, ***et al.*** Luteolin overcomes acquired resistance to osimertinib in non-small cell lung cancer cells by targeting the HGF-MET-Akt pathway. *Am J Cancer Res* 2023, 13: 4145–4162
36. Cai X, Miao J, Sun R, Wang S, Molina-Vila MA, Chaib I, Rosell R, ***et al.*** Dihydroartemisinin overcomes the resistance to osimertinib in EGFR-mutant non-small-cell lung cancer. *Pharmacol Res* 2021, 170: 105701
37. Yao J, Lu Y, Jiao L, Bi L, Yang W, Su L, Shi J, ***et al.*** Chinese herbal medicine (Yiqi-Yangyin-Jiedu decoction) combined with osimertinib as First-Line treatment in EGFR mutation-positive advanced non-small-cell lung cancer (CATLA-2): a study protocol for a double-blind randomized controlled trial. *Front Pharmacol* 2022, 13: 840889
38. Sun Q, Gong T, Liu M, Ren S, Yang H, Zeng S, Zhao H, ***et al.*** Shikonin, a naphthalene ingredient: therapeutic actions, pharmacokinetics, toxicology, clinical trials and pharmaceutical researches. *Phytomedicine* 2022, 94: 153805
39. Xu X, Kalambhe DR, Yu Y, Yu L, Gu Z, Jin X, Wang H, ***et al.*** Co-delivery of shikonin and JQ1 inhibits triple-negative breast tumor progression and lung metastasis through inhibition of epithelial-mesenchymal transition and vasculogenic mimicry. *Acta Pharmacol Sin* 2025, 46: 3314–3326
40. Wang Z, Shen N, Wang Z, Yu L, Yang S, Wang Y, Liu Y, ***et al.*** TRIM3 facilitates ferroptosis in non-small cell lung cancer through promoting SLC7A11/xCT K11-linked ubiquitination and degradation. *Cell Death Differ* 2024, 31: 53–64
41. Cai S, Zhang B, Huang C, Deng Y, Wang C, Yang Y, Xiang Z, ***et al.*** CTRP6 protects against ferroptosis to drive lung cancer progression and metastasis by destabilizing SOCS2 and augmenting the xCT/GPX4 pathway. *Cancer Lett* 2023, 579: 216465
42. Wang L, Fu H, Song L, Wu Z, Yu J, Guo Q, Chen C, ***et al.*** Overcoming AZD9291 resistance and metastasis of NSCLC via ferroptosis and multitarget interference by nanocatalytic sensitizer plus AHP-DRI-12. *Small* 2023, 19: e2204133
43. Liu ZH, Dai XM, Du B. Hes1: a key role in stemness, metastasis and multidrug resistance. *Cancer Biol Ther* 2015, 16: 353–359
44. Yuan Q, Chen X, Han Y, Lei T, Wu Q, Yu X, Wang L, ***et al.*** Modification of α2,6-sialylation mediates the invasiveness and tumorigenicity of non-small cell lung cancer cells *in vitro* and *in vivo* via Notch1/Hes1/MMPs pathway. *Intl J Cancer* 2018, 143: 2319–2330
45. Bousquet Mur E, Bernardo S, Papon L, Mancini M, Fabbrizio E, Goussard M, Ferrer I, ***et al.*** Notch inhibition overcomes resistance to tyrosine kinase inhibitors in EGFR-driven lung adenocarcinoma. *J Clin Invest* 2020, 130: 612–624
46. Sun L, Ke J, He Z, Chen Z, Huang Q, Ai W, Wang G, ***et al.*** HES1 promotes colorectal cancer cell resistance To 5-Fu by inducing Of EMT and ABC transporter proteins. *J Cancer* 2017, 8: 2802–2808
47. Zhang B, Dong S, Wang J, Huang T, Zhao P, Xu J, Liu D, ***et al.*** NOTCH4ΔL12_16 sensitizes lung adenocarcinomas to EGFR-TKIs through transcriptional down-regulation of HES1. *Nat Commun* 2023, 14: 3183
48. Cui M, Ding X, Jiang Y, Zhang L, Cao W, Wang Y, Sheng Z, ***et al.*** PDGFC secreted by cancer-associated fibroblasts promotes epithelial-mesenchymal transition and immunosuppression in lung adenocarcinoma. *Acta Biochim Biophys Sin* 2025, 57: 1625–1635
49. Wang L, Liu Y, Du T, Yang H, Lei L, Guo M, Ding HF, ***et al.*** ATF3 promotes erastin-induced ferroptosis by suppressing system Xc. *Cell Death Differ* 2020, 27: 662–675
50. Lu S, Wang X, He C, Wang L, Liang S, Wang C, Li C, ***et al.*** ATF3 contributes to brucine-triggered glioma cell ferroptosis via promotion of hydrogen peroxide and iron. *Acta Pharmacol Sin* 2021, 42: 1690–1702